SeaFOAM: A Year-Long DAS Deployment in Monterey Bay, California

Barbara Romanowicz*[1], Richard Allen[1], Knute Brekke[2], Li-Wei Chen[1], Yuancong Gou[1], Ivan Henson[1], Julien Marty[1], Doug Neuhauser[1], Brian Pardini[1], Taka'aki Taira[1], Stephen Thompson[1], Junli Zhang[1], and Stephane Zuzlewski[1]

Abstract

Distributed acoustic sensing (DAS) is being explored in a variety of environments as a promising technology for the recording of seismic signals in dense array configurations. There is a particular interest for deploying DAS arrays on the ocean floor, presenting formidable challenges for conventional seismology. Taking advantage of the availability of a dark fiber on the Monterey Bay Accelerated Research System (MARS) 52 km offshore cable at Monterey Bay, California, in July 2022, we installed a DAS interrogator at the shore end of the cable with the intention of acquiring continuous data for a period of one year. Here, we describe the experiment and present examples of observations over the first six months of the deployment.

Cite this article as Romanowicz, B., R. Allen, K. Brekke, L.-W. Chen, Y. Gou, I. Henson, J. Marty, D. Neuhauser, B. Pardini, T. Taira, *et al.* (2023). SeaFOAM: A Year-Long DAS Deployment in Monterey Bay, California, *Seismol. Res. Lett.* **94**, 2348–2359, doi: 10.1785/0220230047.

Introduction

Distributed acoustic sensing (DAS) is an emerging geophysical technology that provides axial strain measurements along fiber-optic cables by sensing optoelectronic signals (Zhan, 2020; Lindsey and Martin, 2021), turning any pre-existing cable into a dense array of one-component broadband strain sensors with meter-scale resolution in a relatively affordable way. DAS was developed by the oil and gas industry (Farhadiroushan *et al.*, 2009; Daley *et al.*, 2013) and more recently has been used on land for global- and crustal-scale seismology (e.g., Lindsey *et al.*, 2017; Jousset *et al.*, 2018; Lellouch *et al.*, 2019; Ajo-Franklin *et al.*, 2019; Yu *et al.*, 2019). Recently, it has started to be deployed in the marine environment. Most permanent broadband seismic stations are installed on land, given the difficult logistics and higher cost of ocean deployment and despite the many efforts in the last 40 yr to deploy seismic observatories in the oceans (H20, ION, OSN… Le Pichon, 1987; Purdy and Dziewonski, 1988; Forsyth *et al.*, 1995; Montagner and Lancelot, 1995; Collins *et al.*, 2001; Suyehiro *et al.*, 2006), including cabled observatories (e.g., Kawaguchi *et al.*, 2007; Barnes *et al.*, 2008; Kanazawa, 2013; Smith *et al*, 2018; S-net, ALOHA) and recent efforts at floating arrays of hydrophones (e.g., Sukhovich *et al.*, 2015) and large aperture seafloor broadband seismic arrays (e.g., PacificArray, Kawakatsu *et al.*, 2019). Although there are still many issues with DAS instrumentation, such as the cost of the instrument, single component recording, and poor characterization of the instrument response, DAS provides a complementary and potentially unprecedented opportunity to instrument the oceans, which cover more than 70% of the Earth's surface, using existing submarine cables and filling gaps in seismic observations offshore.

DAS deployments are flourishing on land, providing valuable information on signal resolution, background noise, instrument response, and calibration under various installation conditions (Wang *et al.*, 2018; Lindsey *et al.*, 2020; Paitz *et al.*, 2021; Muir and Zhan, 2022). Recent DAS studies on submarine cables demonstrate promising data fidelity showing detections of local and teleseismic events, as well as microseisms, infragravity waves, and other oceanic signals spanning a broad frequency range (Lindsey *et al.*, 2019; Sladen *et al.*, 2019; Williams *et al.*, 2019; Lior *et al.*, 2021). However, most of the experiments are short term (lasting a few days to a few weeks) and lack systematic assessment of the instrument response; background noise and its seasonal variations; and, more generally, instrument capability. Here, we describe and illustrate data from an on-going DAS experiment on the Monterey Bay Accelerated Research System (MARS) cable in Monterey Bay, California, that has been deployed for a duration of one yr, starting on 21 July 2022.

1. Berkeley Seismological Laboratory, University of California, Berkeley, California, U.S.A., https://orcid.org/0000-0002-6208-6044 (BR); https://orcid.org/0000-0003-4293-9772 (RA); https://orcid.org/0000-0002-9403-4505 (L-WC); https://orcid.org/0000-0001-6313-0564 (YG); https://orcid.org/0000-0002-6170-797X (TT); 2. Monterey Bay Aquarium Research Institute, Moss Landing, California, U.S.A.

*Corresponding author: barbarar@berkeley.edu

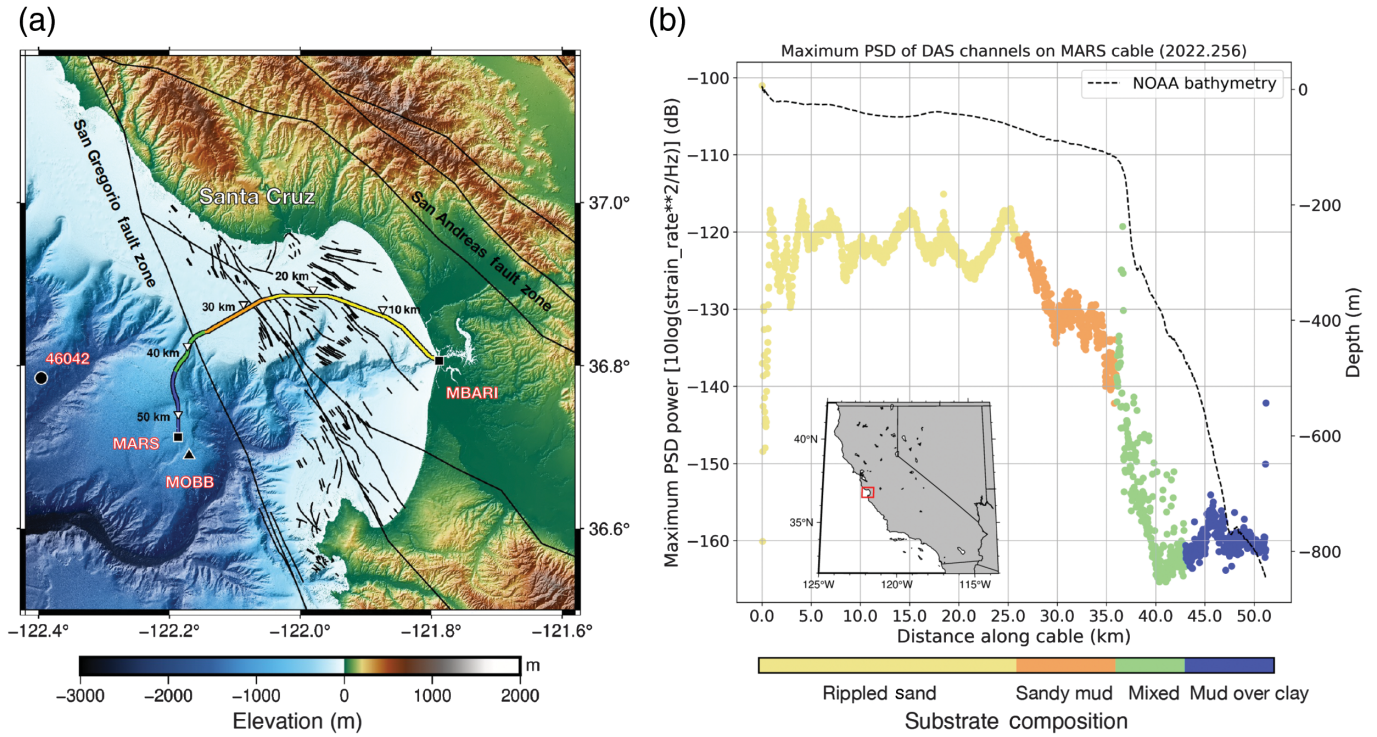

Experimental Setup

The MARS node is located offshore on the west side of the North America–Pacific plate boundary in a seismically active region (Fig. 1). The 52–km-long MARS cable crosses the mostly offshore San Gregorio fault, which is believed to have experienced a magnitude 7+ earthquake after A.D. 1270 (Simpson *et al.*, 1997) and several other poorly documented faults. The 1989 M_L 6.9 Loma Prieta earthquake occurred just north of Monterey Bay. A seafloor very broadband seismic station, MOBB (Romanowicz *et al.*, 2003) was deployed 1.5 km from the MARS node, collecting continuous three-component data until 2014 (in real time from 2009 to 2014; Romanowicz *et al.*, 2009), demonstrating the benefit of offshore stations for the Berkeley Digital Seismic Network (BDSN) earthquake monitoring activities. Although MOBB is not currently operational, its archived data may be valuable as reference for DAS observations.

Taking advantage of a four-day window during the annual MARS node and cable maintenance in 2018, Lindsey *et al.* (2019) installed a DAS interrogator in the MARS shore terminus station, connected it to a single-mode dark fiber inside the MARS cable, while the MARS cabled observatory was unplugged and collected 3.5 TB of DAS data over a 20 km span of the cable. This experiment demonstrated the technical feasibility and intellectual potential of a longer seafloor DAS experiment along the MARS cable. Such an experiment has now been made possible by funding from the National Science Foundation and the availability of a dark fiber on MARS. The goal of the seafloor fiber-optic array in Monterey Bay (SeaFOAM) is to continuously monitor microseismicity, regional or teleseismic earthquakes, ocean currents and waves, and ambient seismic noise, as well as marine mammals like whales or dolphins during a time span of one year. This project also aims to explore the capability of fiber-optic sensing on the ocean floor with data collection in real time.

Figure 1. (a) The location of the Monterey Bay Accelerated Research System (MARS) cable in Monterey Bay, California. The distributed acoustic sensing (DAS) recording extends from the shore station at MBARI to the MARS node, for a distance of 52 km, ranging from very shallow water to water depths in excess of 850 m. Known offshore faults are indicated. The location of NOAA buoy 46042 and of the three-component very broadband buried MOBB seismic station is also shown, ~1500 m south of the MARS node, at a water depth of 1000 m. Continuous three-component broadband data acquired at MOBB from 2003 to 2016 on a CMG-3T instrument are available through the Northern California Earthquake Data Center (NCEDC). (b) Water depth profile along the cable (broken line), showing the location of the steep cliff at a distance of 37 km from shore. The maximum noise power spectral density (PSD; Julian day 2022.256) in the 1–100 s frequency band is also shown, color coded by the type of soil in which the cable resides. Note that 87% of the cable is buried beneath the seafloor, except over the cliff. The water depth effect dominates the PSD level. Inset shows the location of the map in panel (a) in California.

An Optasense DAS interrogator (model QuantX) was connected to a dark fiber on the 52 km MARS cable Bay, in Monterey Bay, California (Fig. 1). Recording started on 21 July 2022. Data are acquired continuously at a sampling rate

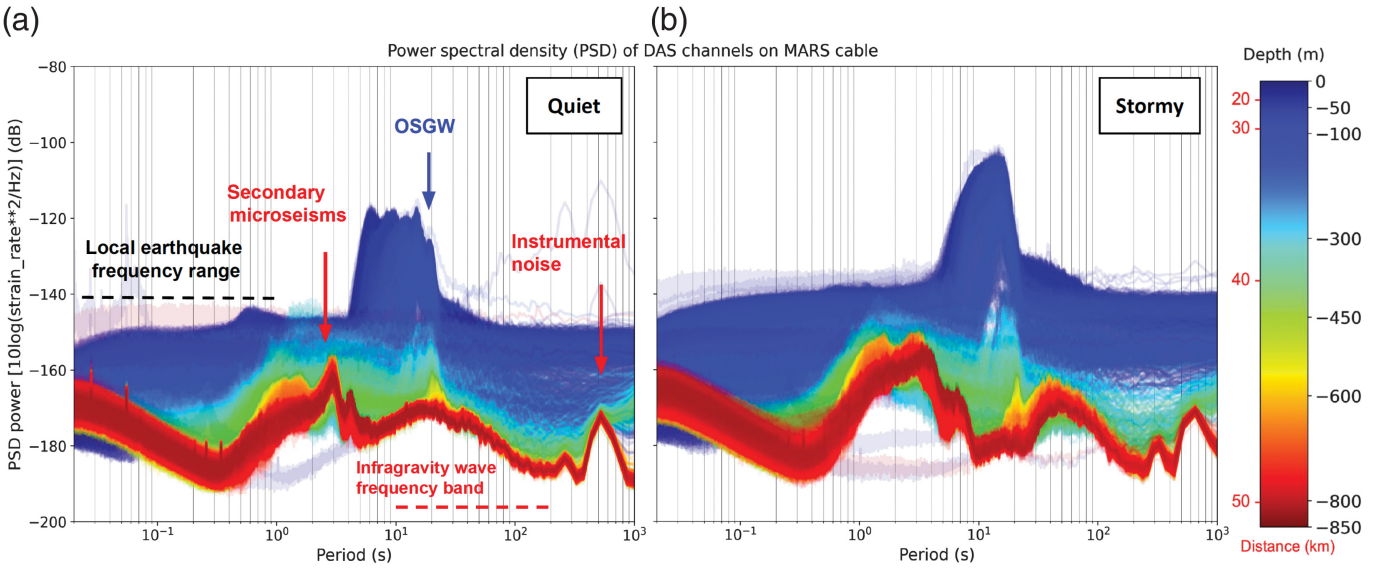

Figure 2. Power spectral density (PSD) of strain rate for every fifth recorded DAS channel on the MARS cable for (a) a quiet day (2022.256) and (b) a stormy day (2023.004). The colors represent the water depth for each channel. The corresponding distance to the shoreline is also indicated on the color bar (red). At all periods, the PSD in shallow water depth (bluish) is higher than in deep water (reddish). The PSD is dominated by ocean surface gravity waves (OSGW) at shallow water depths and by secondary microseisms in deep water and its spectral content changes. Overall spectral energy is higher on a stormy day.

of 200 Hz from 10,245 channels with 5.1 m spacing along the entire length of the cable. After some experimenting, we chose a gauge length of 20.4 m. The corresponding daily DAS archived data volumes average ~360 GB (in HDF5 format). The total volume of data to be archived over the one year deployment is estimated at 130 TB. We have developed a workflow for processing the data in real time. Raw data ("Level 0") are stored on a RAID-6 array of disks at Monterey Bay Aquarium Research Institute (MBARI), whereas spatially decimated data with 200 m spacing ("Level 1") and 100 Hz sampling rate are streamed back the Northern California Earthquake Data Center at the Berkeley Seismological Laboratory for real-time earthquake monitoring activities.

At the time this article was submitted, we have recorded 209 days of data, allowing us to start exploring the capabilities and limitations of the system. More than 100 local and teleseismic events have been detected, including the 25 October 2022 M_w 5.1 earthquake that was widely felt in the San Francisco Bay area. The smallest detected event is a local M_L 2.0 earthquake. This was obtained by estimating the arrival times of *P* waves on the DAS for earthquakes in the U.S. Geological Survey catalog and matching them to peaks in the data using an empirical *P*-wave velocity in the region of 5.60 km/s. This average apparent *P*-wave velocity was estimated from the analysis of all M_L 4+ events recorded on the nearby very broadband ocean bottom station MOBB (Fig. 1; Romanowicz *et al.*, 2003, 2009), within a radius of 100 km of MOBB. A more sophisticated approach to detect local earthquakes on SeaFOAM, potentially complementing the existing catalog, is currently being developed.

Data Clipping

DAS data clipping and the resulting cycle skipping is a common issue resulting from abrupt phase shifts during intense ground motion, such as that caused by nearby seismic activity, but not only. However, when first analyzing data, we observed frequent wrapping of the signal phase in random isolated channels in the absence of significant ground shaking. We think this may be attributed to baseline drift caused by instrumental issues that cause amplitude overflow. We have been able to successfully correct for this cycle skipping automatically; our approach is described in Figure A1.

Background Noise

The depth of water varies significantly along the 52 km of the cable (Fig. 1). For the first ~35 km (distance along the cable from shore), the cable is buried at very shallow water depth (<150 m). It then drops ~150 m over a steep cliff and continues on a smooth ridge, reaching a depth of water of 850 m at the MARS node (e.g., Kuhnz *et al.*, 2020). The cable is buried along almost its entire length, except where it is hanging over the cliff. The character of the background noise varies accordingly with much higher noise in shallow water (Fig. 2). Interestingly, the power spectral density (PSD) is dominated by noise in the ocean surface gravity waveband (OSGW; e.g., Guerin *et al.*, 2022; Williams *et al.*, 2022) at shallow depths (Fig. 2). At larger

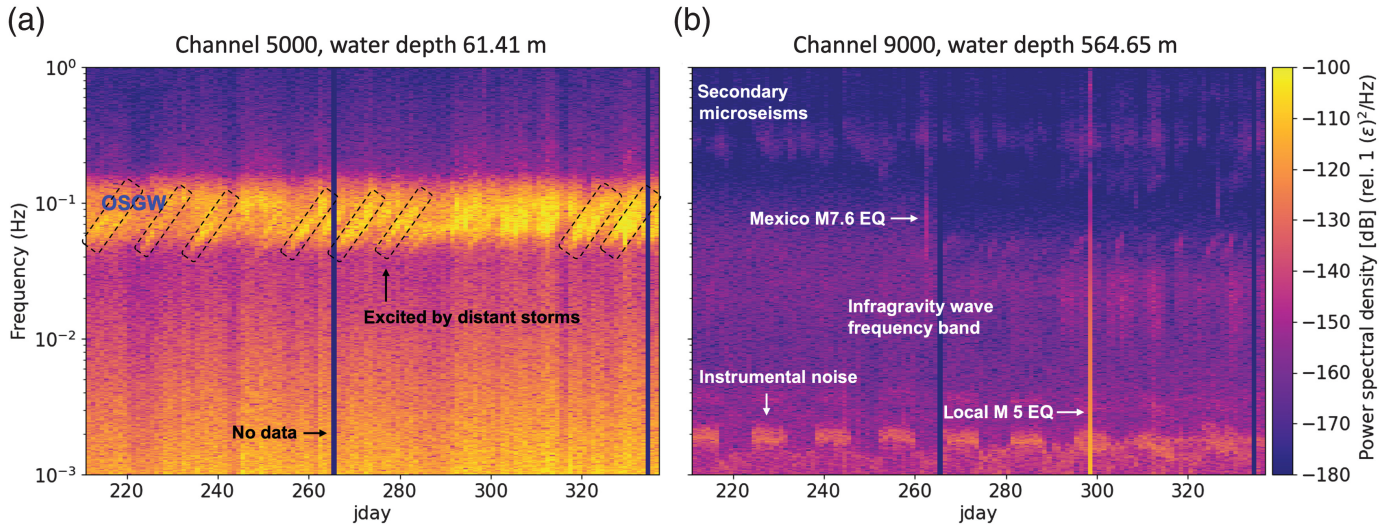

Figure 3. Spectrograms for DAS channels at different distances from shore: (a) 25 km and (b) 45 km using the same color scale. The black lines indicate days with missing data: the interrogator swap on day 265 and the OPTASENSE license renewal on day 334. (a) The ocean surface gravity waves (OSGW) consistently dominate (range 0.05–0.15 Hz), and we observe many dispersed swell arrivals (dashed boxes), excited by distant storms (e.g., Dolenc *et al.*, 2005). (b) Here, secondary microseisms can be observed in the frequency range 0.2–0.4 Hz. The narrow broadband peak observed on day 298 corresponds to a local M_w 5 earthquake, whereas on day 262, an M_w 7.6 teleseismic event occurred in Mexico. The interrogator swap on day 263 resulted in a slight decrease of noise, most notable around 20–30 s period. The infragravity wave energy level (in the frequency band at 0.01–0.06 Hz) gradually increases after day 290 because of the onset of winter stormy weather.

water depths, this is gradually reduced to lower amplitudes and a narrower frequency band, likely caused by hydrodynamic filtering. Over the last 15 km of the cable, which corresponds to depths of water >600 m, the dominant noise is in the secondary microseism band. This is also clearly visible in Figure 3 in which spectrograms are compared for a shallow and a deep channel for the same time period.

Automatic spike detection algorithm and real-time data processing

To help us sort through the large amount of data generated on the DAS and extract events of interest (not only earthquakes), we first designed a simple automatic spike detector. We use the volume size of the raw 1 min compressed HDF5 files containing all of the "level 0" data and applying a spike detection scheme, which is very fast (Fig. 4). The detected spikes (dark inverted triangles) correspond to seismic events and other sudden disturbances that result in an increased volume of recorded data. Although this spike detector only has 1 min temporal resolution and likely misses some small local earthquakes at magnitudes lower than M_L 2, it provides a convenient means for identifying larger events of interest (seismic or other) for further analysis. Subsequently, we illustrate some of the events thus detected, which include strong ocean currents, *T* phases from distant earthquakes, human activities, and vocalizations of whales and such. Only ~82 of the ~476 registered spike detections in the first six months were identified as earthquakes.

In parallel, a pipeline was developed to process Level 1 data in real time. The main program reads the 256 channel 100 samples/s Level 1 CBT30 formatted DAS data from a port on the remote acquisition machine and streams them in real time to our processing center on the Berkeley campus. A subset of the channels are converted to Earthworm (Johnson *et al.*, 1995) Tracebuf2 packets that are inserted into an Earthworm memory ring. This makes them available for inclusion in many real-time processing applications, including the ShakeAlert earthquake early warning (EEW) system (Kohler *et al.*, 2020). Currently, these channels are being processed by an instance of the Earthquake Point-source Integrated Code (EPIC) (formally known an ElarmS; Chung *et al.*, 2019) EEW waveform processor that has been configured with an appropriate filter band and short-term average to long-term average level to detect triggers. These triggers are forwarded to an EPIC event associator in which they are used along with triggers from other seismic stations to detect local earthquakes. These instances of EPIC are for research purposes and not part of the public alerting system today. To date, this real-time EPIC has associated DAS triggers with five events with magnitudes M_L 3.1–3.9 and distances of 27–90 km. In a waveform replay of the data from the 20 December 2022 M_L 6.4 Ferndale event, EPIC also associated DAS triggers with the event at a distance of 467 km. This analysis is very preliminary.

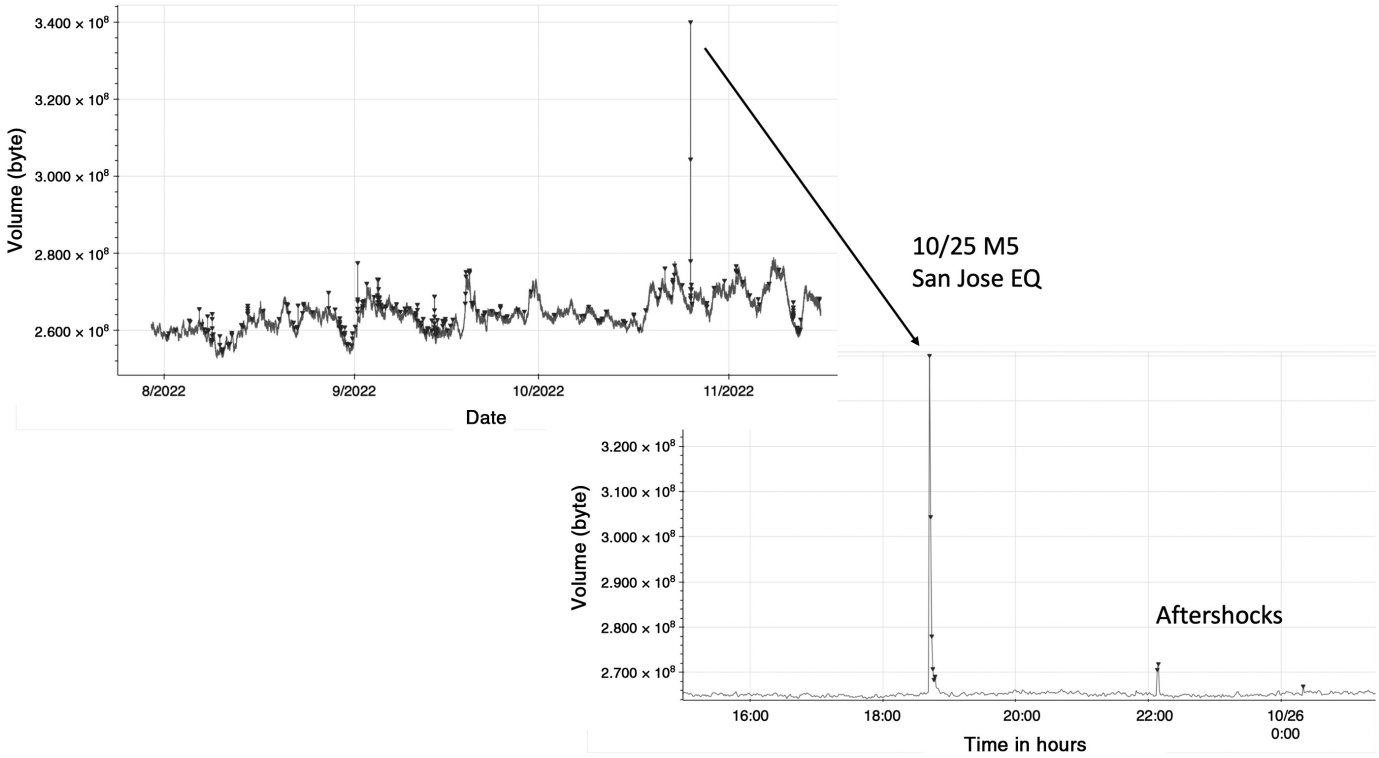

Figure 4. Example of automatic event detection around the time of the 25 October 2022 M_w 5 San Jose earthquake. The mainshock produced a very large spike, and some aftershocks are also visible. The largest spike before the San Jose earthquake corresponds to a nearby M_w 4 earthquake that occurred on 1 September 2022, 5 km east-northeast of Pinnacles, California. The detection works as follows: we first process the data sampled at 1 sample/min and remove long wavelength fluctuations. We then compute the average amplitude and standard deviation for each 100 min moving window. If the amplitude of any point exceeds 3.6 standard deviation on top of the average within each window, the data point is identified as a spike.

Examples of detected events

In Figures 5–7, we present examples of different types of events observed on SeaFOAM so far. Figure 5a shows the record section of a small M_L 2.7 local earthquake on the San Andreas fault with clear *P* and *S* detections up to 20 Hz frequency. A comparison of the strain record at channel 9000 (at large water depth) with a nearby onshore shows comparable signal-to-noise ratio (Fig. 5b,c). Figure 6 shows the record section for the 19 September 2022 M_w 7.6 Mexico earthquake, filtered to highlight surface waves, well recorded along the entire cable, as well as a comparison of the strain record at channel 9000 and the corresponding velocity record at BDSN station FORD, for this event. In Figure 7, we present a record section, high-pass filtered at 2 Hz, showing the *T* phase generated by the 4 September 2022 M_w 6.2 south Pacific earthquake, visible in parts of the cable corresponding to water depths >400 m, which sense the SOFAR channel. In fact, *T* phases are consistently observed on the deeper part of the cable, from large earthquakes in the south and southwest Pacific as illustrated in Figure 8. The corresponding great circle paths arrive on the cable with favorable backazimuths for detecting axial strain from these acoustic waves. Figure 9 shows the detection on 28 September 2022 of one or several high-frequency source(s), which generate Scholte waves propagating along the seafloor interface. The frequency is too low for whale calls. The origin of these signals is yet unknown, but probably, they are caused by local impacts on the seafloor, such as fishing activities such as trawling or the use of heavy fishing gear such as bottom-set longlines, traps, and nets.

Observations of winter storms

As seen in the comparison of PSD on a quiet and stormy day in Figure 2, the DAS records contain rich information about the effects of storms on the background noise at the seafloor. A series of large storms hit the California coast from the West in late December 2022 and January 2023. Figure 10a shows a spectrogram recorded at a deep water DAS channel for the time period 28 December 2022–23 January 2023 in which the onset of the storm that started on 23 December 2022 is clearly visible in the increased level of noise both in the microseism band (1–10 s period) and in the infragravity wave-band (30–100 s period). The filtered DAS record around 0.02 Hz (50 s period) in Figure 10b, whereas spectral wave density (SWD) and significant wave height, SWH, at nearby NOAA buoy 46,042 are shown in Figure 10c,d, respectively.

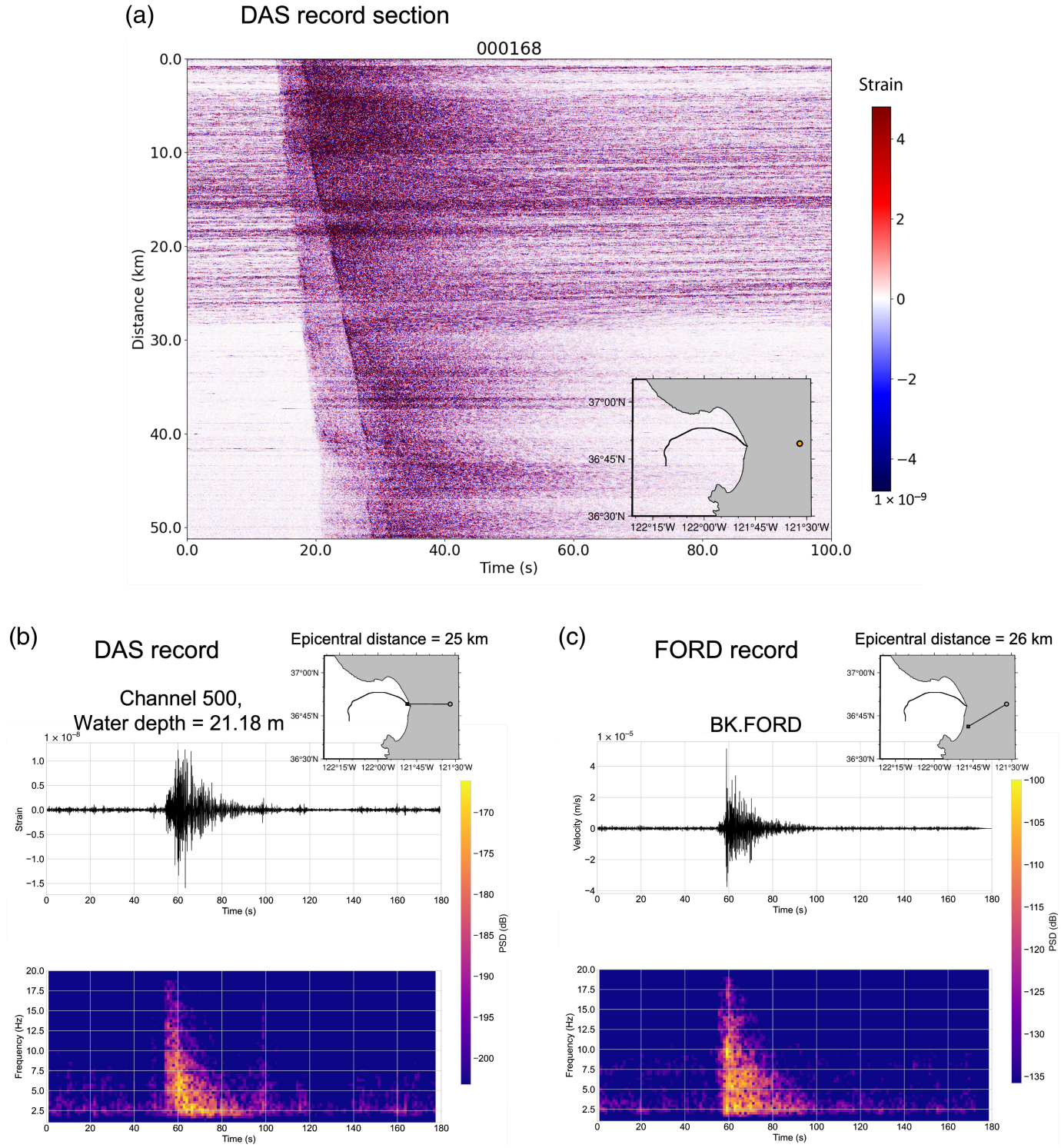

Figure 5. (a) Example of recording of a small local earthquake: the 12 November 2022 M_L 2.7 earthquake on the San Andreas fault. (b) DAS record section in units of strain of all the 10,245 channels after high-pass filtering at 2 Hz. The inset shows the location of the epicenter with respect to the cable. The cable position origin (0 km) is at the shoreline. *P* and *S* arrivals are clearly seen. Note that clear *P*- and *S*-wave arrivals can be observed up to 20 Hz. DAS recording at channel number 500 and corresponding spectrogram in units of strain. (c) Broadband seismic record at on land station FORD (location indicated by a square in inset) and corresponding spectrogram in units of ground velocity. The horizontal components have been rotated into the cable azimuth at channel number 500. The insets in panels (b) and (c) show the Monterey Bay coastline, the location of the cable in the Bay, the event location (open circle), and the location of the DAS channel presented in (b) and of the station presented in (c) (black squares). The color version of this figure is available only in the electronic edition.

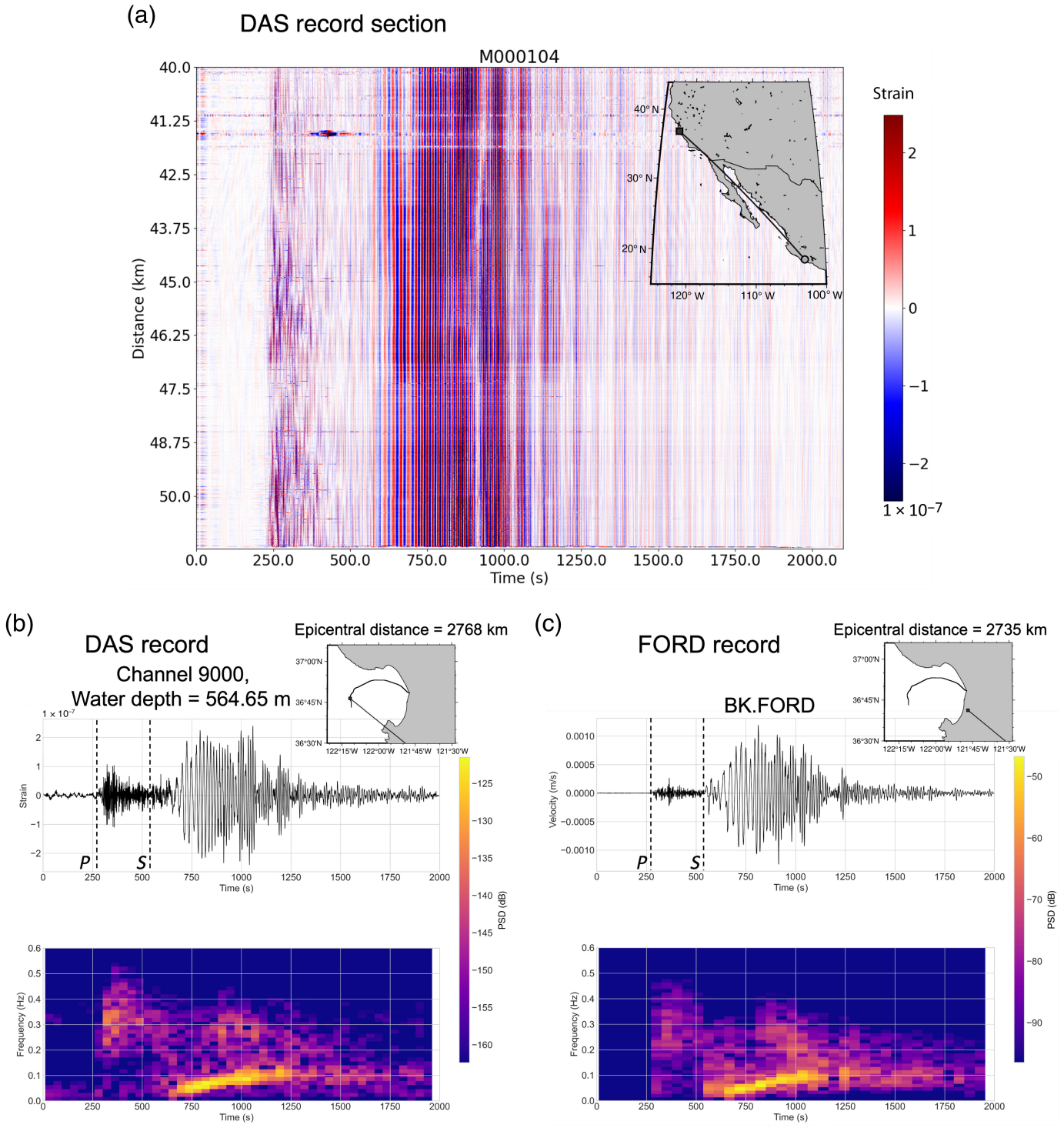

Figure 6. (a) DAS recordings (in units of strain) of the 19 September 2022 M_W 7.6 Mexico earthquake for channels 8,000–10,245 after band-pass filtering between 0.01 and 0.5 Hz. (b) DAS recording of the Mexico event shown in Figure 7 at channel number 9000 (cable distance 45 km and water depth 564.65 m) in units of strain and corresponding spectrogram. (c) Seismogram recorded at on land Berkeley Digital Seismic Network (BDSN) station FORD in units of velocity rotated into cable azimuth at the on land station FORD and corresponding spectrogram. Note the well-matched recording of fundamental mode and overtone surface wave energy. In panels (b) and (c), we have indicated the predicted arrival times of *P* and *S* waves, computed in the Preliminary Reference Earth model (PREM) (Dziewonski and Anderson, 1981). The insets in panels (b) and (c) show the Monterey Bay coastline, the location of the cable in the Bay, the event location (open circle), and the location of the DAS channel presented in (b) and of the station presented in (c) (black squares). The color version of this figure is available only in the electronic edition.

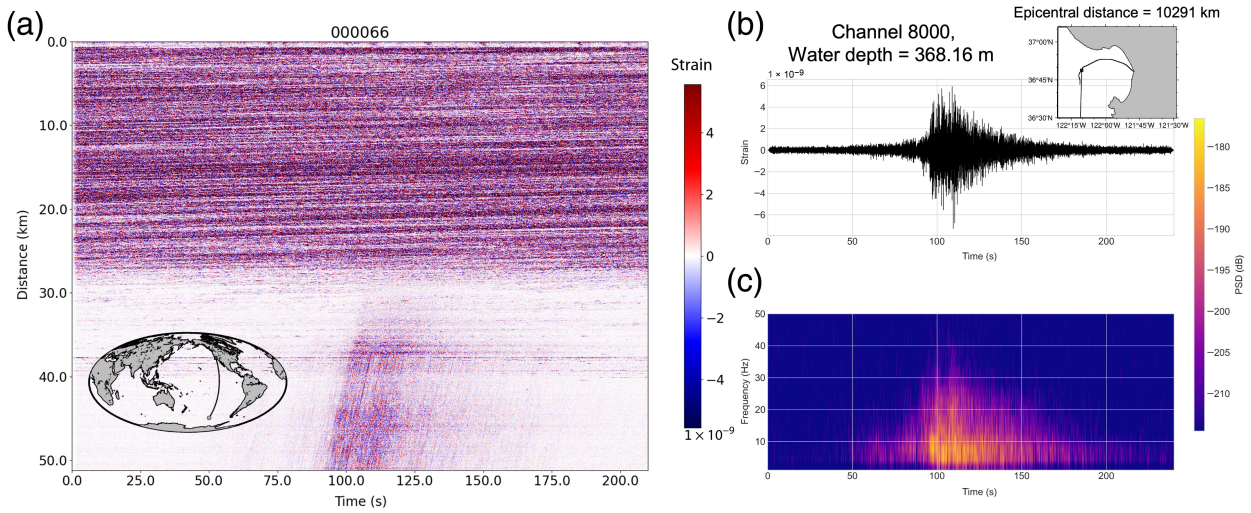

Figure 7. (a) DAS recordings (in units of strain) of the 4 September 2022 M 6.2 Southern East Pacific Rise earthquake (epicentral distance = 10,291 km) for all the 10,245 channels after high-pass filtering at 2 Hz. (b) The DAS observations and spectrogram at the location of channel number 8000 (cable distance 40 km and water depth 368.16 m). The *T* waves travel with an apparent velocity of 1.5 km/s along the cable, which is consistent with the velocity of an acoustic wave propagating in water. Panel (c) shows the spectrogram corresponding to panel (b). The inset map in panel (a) shows the great circle path from the event (open circle) to the DAS cable (black square). The inset in panel (b) is a blow up of the map in panel (a) showing the location of channel 8000 on the DAS cable and a portion of the great circle path between the event and channel 8000. The color version of this figure is available only in the electronic edition.

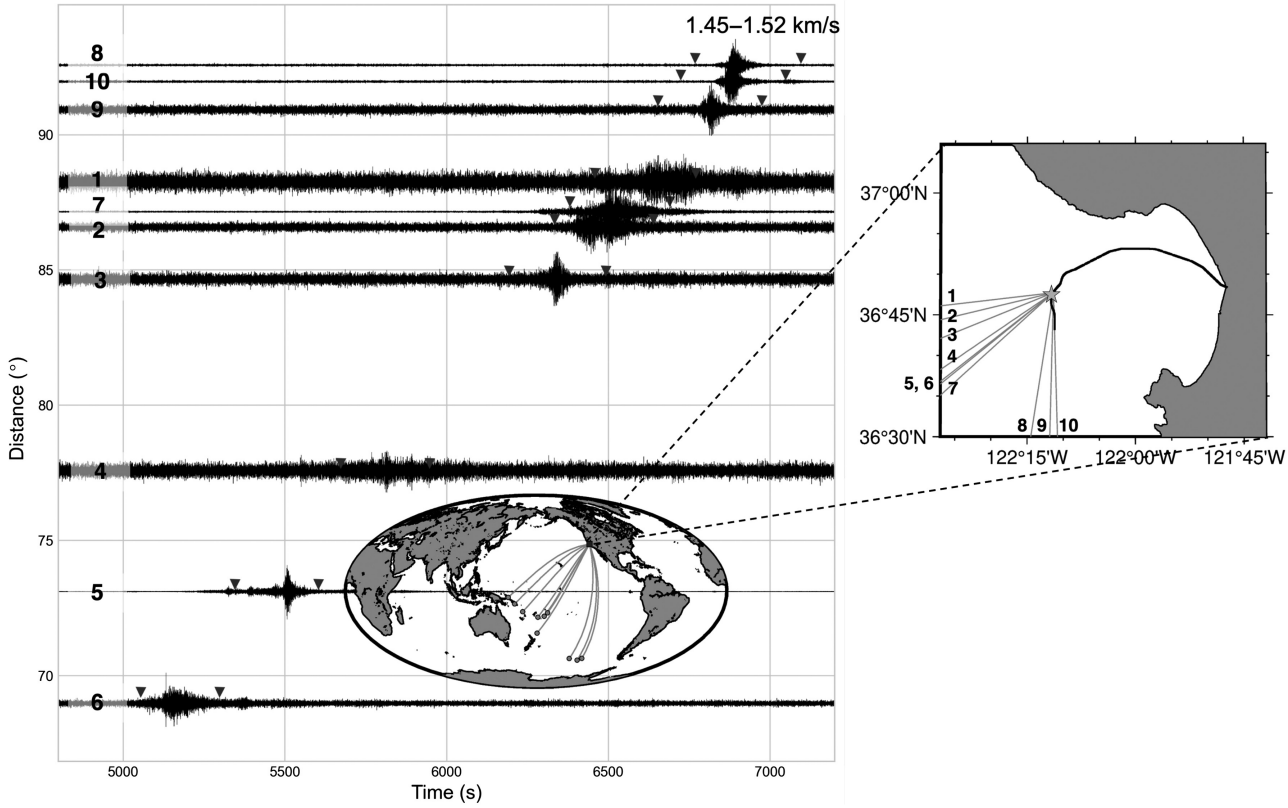

Figure 8. DAS recordings at the location of channel number 8500 (depth of water = 452.52) of multiple M_L 5.8–7.3 teleseismic events aligned by epicentral distance. The triangles mark the apparent velocity range of 1.45–1.52 km/s, which is consistent with a propagation path entirely in the water along the great circle paths from the epicenters (open circles) to the MARS cable shown in a global map in the inset, and in zoomed view around Monterey Bay on the right. Note that *T* waves are observed mostly for earthquakes in the southwest Pacific.

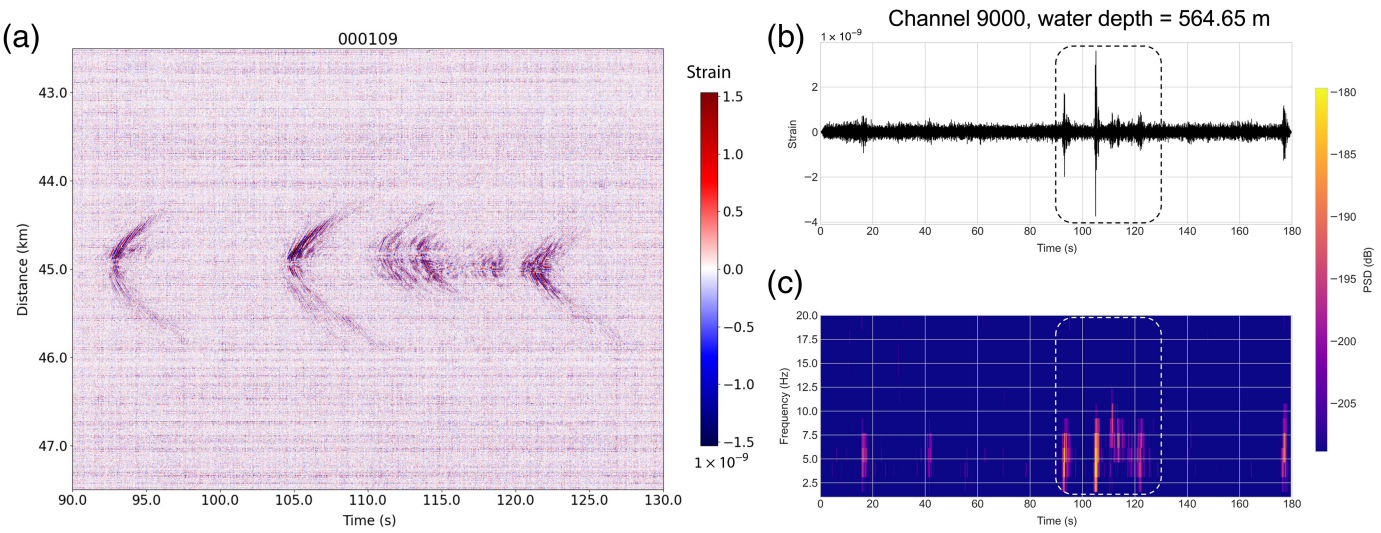

Figure 9. (a) DAS recordings (in units of strain) of a series of events on 28 September 2022 for the 8500–9500 channels after high-pass filtering at 2 Hz that correspond to unidentified sources. (b,c) The dashed boxes highlight the DAS observation and spectrogram at the location of channel number 9000 (cable distance 45 km and water depth 564.65 m). The seismic energy asymmetrically propagates outward with an apparent velocity of 200–300 m/s which likely corresponds to fundamental-mode Scholte waves. The color version of this figure is available only in the electronic edition.

The DAS clearly tracks the fluctuations in the storm energy as recorded in the buoy data. Interestingly, the double-frequency microseismic noise maximum period fluctuates in time and closely tracks the longest period in the SWD record. Investigating the relationship in time, frequency, and amplitude of the strain records along the cable in the microseismic and infragravity wavebands with those of the causative storms may lead to improved understanding on the generation of the former in this near-coast environment (e.g., Smit *et al.*, 2018).

Conclusions and Future Plans

The location of the MARS cable on the seafloor provides a great opportunity to investigate the coupling mechanisms between ocean waves and the seafloor temporally and spatially using seafloor DAS. We observe OSGW and secondary microseisms, infragravity waves, dispersed swell arrivals, and instrumental noise. We also observe several seismic events, including regional, teleseismic earthquakes, and *T* waves from teleseismic events, as well as some yet unidentified signals that may originate from marine mammals.

In addition to these observations, which we continue to investigate, the submarine DAS deployment could be valuable for enhancing earthquake monitoring efforts, including EEW for offshore events. EEW is powered by rapid earthquake source parameter estimation algorithms, which require seismic sensors near to the epicenters. Harnessing seismic observations from offshore fibers could facilitate and improve EEW systems around the globe (Allen and Melgar, 2019), including the ShakeAlert EEW system in the United States (Kohler *et al.*, 2020). One of our goals is to fully integrate the Level 1 DAS data into the real-time seismic monitoring system in northern California, including the EEW system. We are currently developing earthquake detection algorithms based on DAS data, including seismic phase picking, earthquake location, and magnitude estimation.

Data and Resources

Figures were drawn using PyGMT available at https://www.pygmt.org/v0.4.0 (last accessed May 2023), a wrapper around Generic Mapping Tools version 6 (GMT6; Wessel *et al.*, 2019). All data shown in this article are from the distributed acoustic sensing (DAS) deployment it describes.

Declaration of Competing Interests

The authors acknowledge that there are no conflicts of interest recorded.

Acknowledgments

This work is supported by National Science Foundation (NSF) Grant Number OCE-2023301 and California Governor's Office of Emergency Services, Agreement Number 6172-2018. Nate Lindsey spearheaded this project while still a graduate student at the University of California, Berkeley, and after moving to Stanford wrote a successful proposal to NSF with Lucia Gualteri and came up with the name seafloor fiber-optic array in Monterey Bay. Greg Beroza is the current Stanford principal investigator on the NSF grant cited earlier. The authors thank Martin Karrenbach and Victor Yatsev of Optasense Inc. for their help installing and configuring the distributed acoustic sensing equipment, Ethan Williams, and an unidentified reviewer for their helpful comments on the initial article.

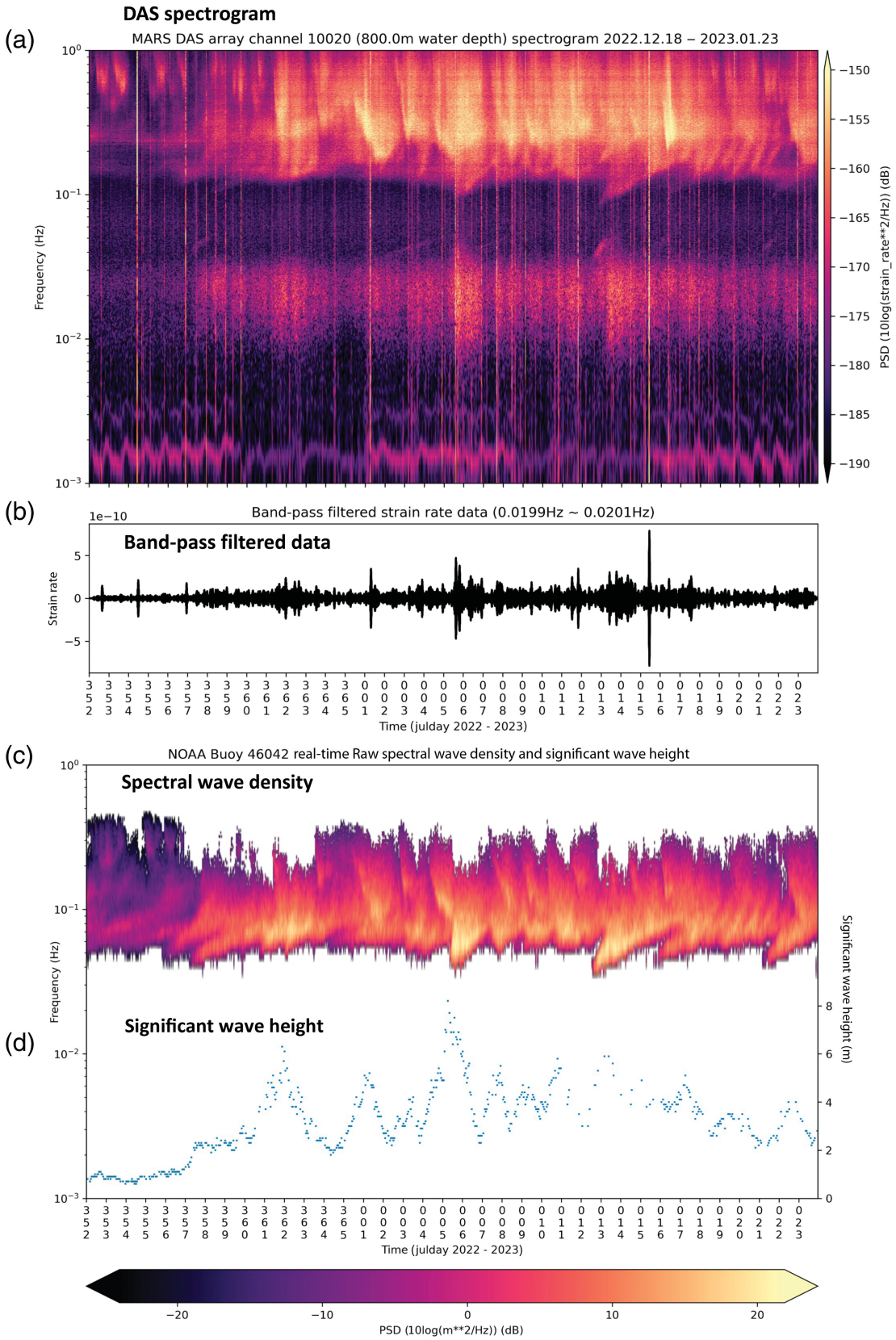

Figure 10. (a) Spectrogram of the DAS recording at channel 10,020 (800 m water depth and 51.1 km along the cable) for Julian day 2022.352–2023.023. (b) Strain rate record, narrow-pass filtered at ~0.02 Hz for the same time interval. (c) Spectral wave density (SWD) and (d) significant wave height (SWH) data recorded at NOAA buoy 46,042 (Fig. 1) for the same time interval. A storm began around 2022.357 as seen in the increase in SWD and SWH at that time, correlated with an increase in noise on the DAS recording both in the microseismic band and in the infragravity waveband (0.01–0.03 Hz). The persistent noise oscillating around 500 s period is of instrumental origin, likely generated by activity at the MARS node.

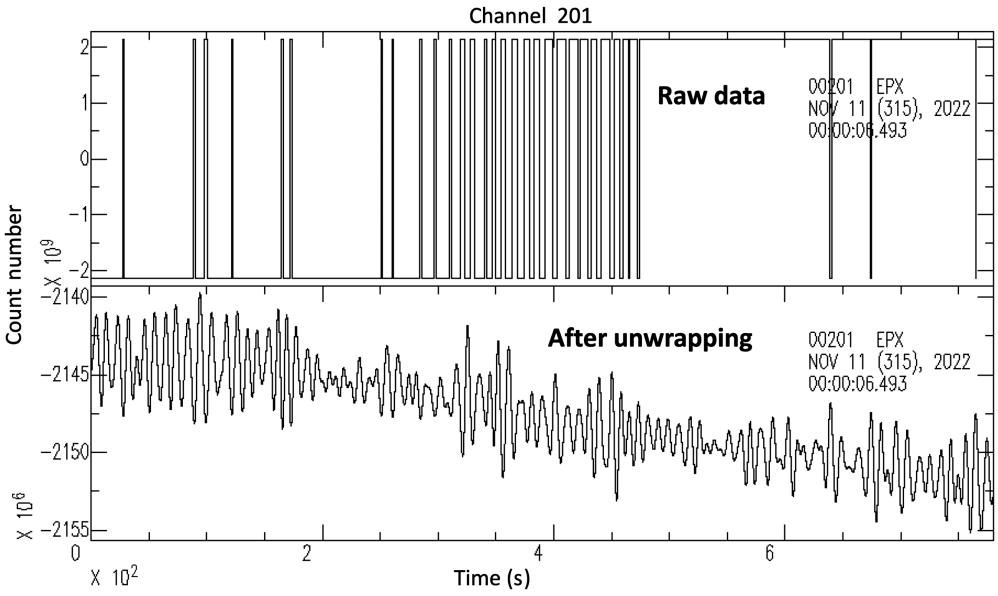

Figure A1. Appendix Signal unwrapping caused by signal saturation on an individual channel. Raw distributed acoustic sensing (DAS) recording on 11 November 2022 for channel 201, showing some saturation, which is caused by the amplitude of the signal exceeding the maximum count number (from $= -2^{31}$ to 2^{31-1}). *X* axis units are in seconds. When this happens, the sign is reversed. Because of the slow drift and known trend, it is sufficient to consider one cycle for unwrapping. We identify the parts in the DAS channel record in which wrapping occurs because of sign flipping and assign them a value of 1 for a change from positive to negative, −1 for a change from negative to positive and 0 if there is no sign flipping. We construct an array with the same length as the DAS record to store this information and then multiply the entire array by the value of 2^{32} (the saturation amplitude), after which we add this array to the DAS record. Detecting the sign reversal and unwrapping restores the continuous time series.

References

Ajo-Franklin, J. B., S. Dou, N. J. Lindsey, I. Monga, C. Tracy, M. Robertson, V. Rodriguez Tribaldos, C. Ulrich, B. Freifeld, T. Daley, *et al.* (2019). Distributed acoustic sensing using dark fiber for near-surface characterization and broadband seismic event detection, *Sci. Rep.* **9,** 1328.

Allen, R. M., and D. Melgar (2019). Earthquake early warning: Advances, scientific challenges, and societal needs, *Annu. Rev. Earth Planet. Sci.* **47,** 361–88.

Barnes, C. R., M. M. R. Best, and A. Zielinski (2008). The NEPTUNE Canada regional cabled ocean observatory, available at https://www.sea-technology.com (last accessed July 2008).

Chung, A. I., I. Henson, and R. M. Allen (2019). Optimizing earthquake early warning performance: ElarmS-3. *Seismol. Res. Lett.* **90,** no. 2A, 727–743, doi: 10.1785/0220180192.

Collins, J. A., F. L. Vernon, J. A. Orcutt, R. A. Stephen, K. R. Peal, F. B. Wooding, F. N. Spiess, and J. A. Hildebrand (2001). Broadband seismology in the oceans: Lessons from the ocean seismic network pilot experiment, *Geophys. Res. Lett.* **28,** 49–52.

Daley, T. M., B. M. Freifeld, J. Ajo-Franklin, S. Dou, R. Pevzner, V. Shulakova, S. Kashikar, D. E. Miller, J. Goetz, J. Henninges, *et al.* (2013). Field testing of fiber-optic distributed acoustic sensing (DAS) for subsurface seismic monitoring, *The Leading Edge* **32,** 936–42.

Dolenc, D., B. Romanowicz, D. Stakes, P. McGill, and D. Neuhauser (2005). Observations of infragravity waves at the Monterey Ocean Bottom broadband station (MOBB), *Geochem. Geophys. Geosyst.* **5,** Q09002, doi: 10.1029/2005/2005GC000988.

Dziewonski, A. M., and D. L. Anderson (1981). Preliminary Reference Earth Model, *Phys. Earth Planet. Inter.* **25,** 297–356.

Farhadiroushan, M., T. R. Parker, and S. Shatalin (2009). Method and apparatus for optical sensing, *WO2010136810A2.*

Forsyth, D., A. Dziewonski, and B. Romanowicz (1995). Scientific objectives and required instrumentation, in *Broadband Seismology in the Oceans: Towards a Five Year Plan*, M. Purdy (Editor), Proceedings of the Ocean Seismic Network Workshop, Joint Oceanographic Institutions, Washington, DC, 8–18.

Guerin, G., D. Rivet, M. P. A. van den Ende, E. Stutzmann, A. Sladen, and J. P. Ampuero (2022). Quantifying microseismic noise generation from coastal reflection of gravity waves recorded by DAS, *Geophys. J. Int.* **231,** 394–407.

Johnson, C., A. Bittenbinder, B. Bogaert, L. Dietz, and W. Kohler (1995). Earthworm: A flexible approach to seismic network processing, *IRIS Newsletter* **14,** no. 2, 1–4.

Jousset, P., T. Reinsch, T. Ryberg, H. Blanck, A. Clarke, R. Aghayev, G. P. Hersir, J. Henninges, M. Weber, and C. M. Krawczyk (2018). Dynamic strain determination using fibre-optic cables allows imaging of seismological and structural features, *Nat. Commun.* **9,** 2509.

Kanazawa, T. (2013). Japan trench earthquake and tsunami monitoring network of cable-linked 150 ocean bottom observatories and its impact to earth disaster science, *Proc. of the 2013 IEEE International Underwater Technology Symposium (UT)*, Tokyo, Japan, 5–8 March 2013, 1–5.

Kawaguchi, K., E. Araki, and Y. Kaneda (2007). A design concept of seafloor observatory network for earthquakes and tsunamis, *Proc. of the International Symposium on Underwater Technology 2007/ International Workshop on Scientific Use of Submarine Cables and Related Technologies 2007*, Tokyo, Japan, April 2007.

Kawakatsu, H., J. B. Gaherty, H. Utada, S. M. Lee, Y. Kim, and Z. Eilon (2019). New progress in building Pacific array: An international collaboration to image mantle dynamic processes across the Pacific basin, *Eos Trans. AGU*, (Fall Meet. 2019), Abstract #DI11A-01.

Kohler, M. D., D. E. Smith, J. Andrews, A. I. Chung, R. Hartog, I. Henson, D. D. Given, R. de Groot, and S. Guiwits (2020). Earthquake early warning ShakeAlert 2.0: Public rollout, *Seismol. Res. Lett.* **91,** 1763–1775, doi: 10.1785/0220190245.

Kuhnz, L. A., K. Buck, C. Lovera, S. Litvin, P. J. Whaling, and J. P. Barry (2020). Potential impacts of the Monterey accelerated research system (MARS) cable on the seabed and benthic faunal assemblages, *MBARI Rept.* 52 pp., doi: 10.13140/RG.2.2.12907.57122.

Le Pichon, (1987). *Report of the Second Conference on Scientific Ocean Drilling (COSOD II)*, Strasbourg, France, 6–8 July 1987.

Lellouch, A., S. Yuan, Z. Spica, B. Biondi, and W. L. Ellsworth (2019). Seismic velocity estimation using passive downhole distributed acoustic sensing records—Examples from the San Andreas Fault observatory at depth, *J. Geophys. Res.* **124,** 6931–6948.

Lindsey, J. N., T. C. Dawe, and J. B. Ajo-Franklin (2019). Illuminating seafloor faults and ocean dynamics with dark fiber distributed acoustic sensing, *Science* **366,** 1103–1107.

Lindsey, N. J., and E. R. Martin (2021). Fiber-optic seismology, *Annu. Rev. Earth Planet. Sci.* **49,** 309–336.

Lindsey, N. J., E. R. Martin, D. S. Dreger, B. Freifeld, S. Cole, S. R. James, B. L. Biondi, and J. B. Ajo‐Franklin (2017). Fiber‐optic network observations of earthquake wavefields, *Geophys. Res. Lett.* **44,** no. 23, 11–792.

Lindsey, N. J., H. Rademacher, and J. B. Ajo-Franklin (2020). On the broadband instrument response of fiber-optic DAS arrays, *J. Geophys. Res.* **125,** e2019JB018145.

Lior, I., A. Sladen, D. Rivet, J. P. Ampuero, Y. Hello, C. Becerril, H. F. Martins, P. Lamare, C. Jestin, S. Tsagkli, *et al.* (2021). On the detection capabilities of underwater distributed acousting sensing, *J. Geophys. Res.* doi: 10.1029/2020JB020925.

Montagner, J. P., and Y. Lancelot (Editors) (1995). *Multidisciplinary Observatories on the Deep Seafloor, Rept. of the International Ocean Network Workshop Held at Marseille*, Institut National des Sciences de l'Univers/Centre National de la Recherche Scientifique, France, 11–13 January 1995, Ocean Drilling Project-France.

Muir, J., and Z. Zhan (2022). Wavefield-based evaluation of DAS instrument response and array design, *Geophys. J. Int.* **229,** 21–34.

Paitz, P., P. Edme, D. Gräff, F. Walter, J. Doetsch, A. Chalari, C. Schmelzbach, and A. Fichtner (2021). Empirical investigations of the instrument response for distributed acoustic sensing (DAS) across 17 Octaves, *Bull. Seismol. Soc. Am.* **111,** 1–10.

Purdy, G. M., and A. M. Dziewonski (1988). Proceedings of a workshop on broad-band downhole seismometers in the deep ocean, Joint Oceanographic Institutions, Inc. and the JOI U.S. Science Advisory Committee, Washington, DC, 105 pp.

Romanowicz, B., P. McGill, D. Neuhauser, and D. Dolenc (2009). Acquiring real time data from the broadband ocean bottom seismic observatory in Monterey Bay (MOBB), *Seismol. Res. Lett.* **80,** 196–204.

Romanowicz, B., D. Stakes, R. Uhrhammer, P. McGill, D. Neuhauser, T. Ramirez, and D. Dolenc (2003). The MOBB experiment: A prototype permanent off-shore ocean bottom broadband station, *Eos Trans. AGU* **84,** 325–332.

Simpson, G. D., S. C. Thompson, J. S. Noller, and W. R. Lettis (1997). The northern San Gregorio fault zone: Evidence for the timing of late Holocene earthquakes near Seal Cove, California, *Bull. Seismol. Soc. Am.* **87,** no. 5, 1158–1170.

Sladen, A., D. Rivet, J. P. Ampuero, L. De Barros, Y. Hello, G. Calbris, and P. Lamare (2019). Distributed sensing of earthquakes and ocean-solid Earth interactions on seafloor telecom cables, *Nat. Commun.* **10,** no. 1, 1–8.

Smit, P. B., T. T. Janssen, T. H. C. Herbers, T. Taira, and B. A Romanowicz (2018). Infragravity radiation across the shelf break, *J. Geophys. Res.* **123,** doi: 10.1029/2018JC013986.

Smith, L. M., J. A. Barth, D. S. Kelley, A. Plueddemann, I. Rodero, G. A. Ulses, M. F. Vardaro, and R. Weller (2018). The ocean observatories initiative, *Oceanography* **31,** 16–35.

Sukhovich, A., S. Bonnieux, Y. Hello, J. O. Irisson, F. J. Simons, and G. Nolet (2015). Seismic monitoring in the oceans by autonomous floats, *Nat. Commun.* **6,** 8027, doi: 10.1038/ncomms9027.

Suyehiro, K., J. P. Montagner, R. A. Stephen, E. Araki, T. Kanazawa, J. Orcutt, B. Romanowicz, S. Sacks, and M. Shinohara (2006). Ocean seismic observatories, *Oceanography* **19,** 104–109.

Wang, H. F., X. Zeng, D. E. Miller, D. Fratta, K. L. Feigl, C. H. Thurber, and R. J. Mellors (2018). Ground motion response to an M_L 4.3 earthquake using co-located distributed acoustic sensing and seismometer arrays, *Geophys. J. Int.* **213,** 2020–2036.

Wessel, P., J. F. Luis, L. Uieda, R. Scharroo, F. Wobbe, W. H. F. Smith, and D. Tian (2019). The generic mapping tools version 6, *Geophys. Res. Lett.* **20,** 5556–5564.

Williams, E. F., M. R. Fernández-Ruiz, R. Magalhaes, R. Vanthillo, Z. Zhan, M. Gonzalez Herraez, and H. F. Martins (2019). Distributed sensing of microseisms and teleseisms with submarine dark fibers, *Nat. Commun.* **10,** no. 1, 1–11.

Williams, E. F., Z. Zhan, H. F. Martins, M. R. Fernández-Ruiz, S. Martín-López, M. González-Herráez, and J. Callies (2022). Surface gravity wave interferometry and ocean current monitoring with ocean-bottom DAS, *J. Geophys. Res.* **127,** e2021JC018375, doi: 10.1029/2021JC018375.

Yu, C., Z. Zhan, N. J. Lindsey, J. B. Ajo-Franklin, and M. Robertson (2019). The potential of DAS in teleseismic studies: Insights from the Goldstone experiment, *Geophys. Res. Lett.* **46,** 1320–1328.

Zhan, Z. (2020). Distributed acoustic sensing turns fiber-optic cables into sensitive seismic antennas, *Seismol. Res. Lett.* **91,** 1–15.

Manuscript received 16 February 2023
Published online 9 June 2023